J. Ocean Univ. China (Oceanic and Coastal Sea Research)
https://doi.org/10.1007/s11802-021-4565-y
ISSN 1672-5182, 2021 20 (4): 755-764
http://www.ouc.edu.cn/xbywb/
E-mail:xbywb@ouc.edu.cn

Studies on the Inversion Phenomenon of Physical Properties Observed in the Huagang Formation Reservoir in the Xihu Sag Based on the Water-Rock Reaction Experiments

HUANG Siqin[1)], XU Fanghao[1), *], XU Guosheng[1)], CUI Hengyuan[1)], and ZHANG Wu[2)]

1) *State Key Laboratory of Oil and Gas Reservoir Geology and Exploitation*, *Chengdu University of Technology*, *Chengdu* 610059, *China*
2) *CNOOC (China) Co*., *Ltd*., *Shanghai Company*, *Shanghai* 200030, *China*

(Received April 17, 2020; revised July 20, 2020; accepted October 27, 2020)

Abstract In the Xihu Sag, the reservoirs of the Paleogene Huagang formation have entered the middle diagenetic stage A and the rock physical properties of the water layer are considerably more suitable for the gas migration and storage than those of the present gas layer, indicating the inversion of the physical properties. In this study, core samples were collected from the corresponding reservoir to conduct water-rock reaction experiments in acidic, alkaline, and neutral systems under the specific temperature and pressure. The reasons for the inversion of physical properties were investigated based on the experiment results in reservoir diagenetic environments. The inversion of physical properties can be attributed to the fact that the diagenetic environment around the gas-water interface controls the water-rock reaction effect. With different types of acidic substances, two different situations corresponding to inverted physical properties were analyzed along with the corresponding mechanisms. When the pore fluid is acidic, the physical properties make the overall water layer a better reservoir space than the gas layer, which can be referred to as the overall inversion of physical properties. When the fluid were generally neutral or weakly alkaline and the gas layer was rich in CO_2, only the physical properties of the water layer adjacent to the gas-water interface were more favorable for the gas migration than those of the gas layer. This phenomenon can be referred to as the near-interface inversion of physical properties.

Key words Xihu Sag; water-rock reaction; reservoir evolution; inverted physical properties; diagenetic environment; special phenomenon

1 Introduction

The prospects of natural gas exploration are excellent in the Xihu Sag, the East China Sea continental shelf basin. Until now, more than ten hydrocarbon-bearing structures have been discovered in this region (Su *et al*., 2014). In the previous century, the reserves of the Xihu Sag have become $2500\times10^8\,m^3$ (Li and Li, 2003). The Paleogene–Oligocene Huagang formation, which is one of the most important production strata of tight sandstone gas in the sag, has become the focus of oil and gas exploration and development in recent years. Majority of the successful oil and gas exploration relies heavily on the discovery of sandstone reservoirs with sufficient porosity and permeability to support commercial development (Taylor *et al*., 2010). Therefore, understanding the reservoir quality is important to achieve successful exploration and is of great significance to study the characteristics of the reservoirs in the Huagang formation of the Xihu Sag. Some reservoir-related phenomena have been discovered in the Huagang formation in recent years. The inverted physical properties of the water and gas layers are considered to be one such phenomenon.

Previous studies have suggested that the distribution of the gas and water layers is generally controlled by the physical properties during the migration and accumulation of natural gas in clastic reservoirs. In good reservoirs with physical properties which have low resistance to fluid migration, natural gases can displace water at a low-pressure threshold, simplifying the charging of natural gas and the formation of gas layers. However, in reservoirs exhibiting poor physical properties, owing to high resistance to fluid migration, natural gas can only begin to displace water at a higher-pressure threshold, so it is difficult for the formation of mixed gas-water layers, gas-containing water layers, and maybe dry layers (Zeng and Wang, 2000; Han *et al*., 2019; He *et al*., 2020). Under normal circumstances, natural gas can be easily distributed through sand bodies with favorable physical properties. Therefore, in the gas

* Corresponding author. E-mail: xufanghao17@cdut.edu.cn

layer the host rocks have more favorable physical properties than in the water layer of the same gas reservoir (Li *et al*., 2017). However, inverted physical properties, when the water layers have more favorable physical properties than the gas layers, can be observed in the gas-bearing structures of the Huagang formation reservoir in the Xihu Sag.

According to the division of diagenetic stages in clastic rocks, oil and gas industry standard of the People's Republic of China (SY/T5477-2003), the reservoirs in the Huagang formation in the Xihu Sag are mainly at middle diagenetic stages A and B and a small number of reservoirs are at the early diagenetic stage. The inversion phenomenon of physical properties can be mainly observed in reservoirs at middle diagenetic stage A, and only minor differences can be observed between the properties of the gas and water layers at middle diagenetic stage B. In Fig.1, the physical properties of the H_3b water layer in the M7 structure are better than those of the gas layer and the physical properties of the lower part are generally better than those of the upper part. A similar phenomenon can also be observed in the M2 structure (Fig.1b). In this study, the M7 structure, which is the most typical structure exhibiting inverted physical properties in the study area, was selected as the study object. In accordance with the basic data related to the physical properties of the rock as well as the lithology, pressure and temperature of the reservoir, the water-rock reaction was experimentally analyzed to study this phenomenon and reveal the mechanism associated with its occurrence.

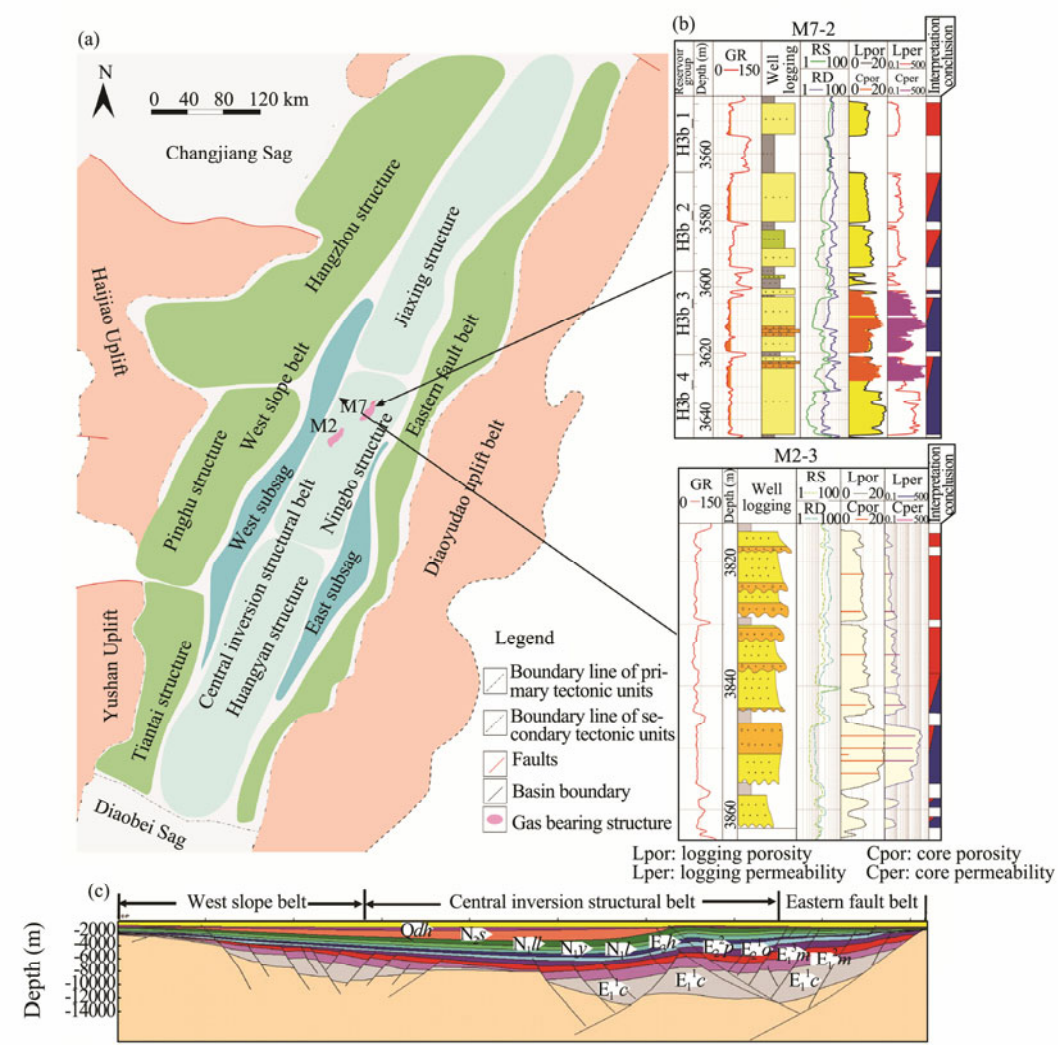

Fig.1 Geological setting of the Xihu Sag, showing inverted physical properties within the reservoir.

2 Geological Setting

The Xihu Sag is located in the middle of the East Zhejiang Depression Belt (124°270′E–127°000′E, 27°300′N–30°590′N) in the East China Sea Shelf Basin. The Xihu Sag is a strike-slip and pull-apart continental margin rift basin located at the Diaoyu Island residual arc (Hu *et al*., 2010; Zhou *et al*., 2018; Liu *et al*., 2019). The basin is bounded by the Diaoyu Island fold belt on the east and the uplifted sea reef on the west. In the south, the Xihu Sag is connected to the Diaobei Depression, whereas it is connected to the Fujiang Depression in the north. The Xihu Sag is about 440 km from north to south and 110 km from east to west, with a total area of approximately 4.27×10^4 km^2 (Yang *et al*., 2009; Hao *et al*., 2018). The sag has

a diamond-like shape, with a clear pattern of east–west zonation and north–south blocking (Dai *et al*., 2014; Zhang *et al*., 2014; Li *et al*., 2016; Wang *et al*., 2017) (Fig.1a).

The sedimentary basement within the Xihu Sag comprises Cretaceous volcanic rocks and Cenozoic sedimentary rocks. The Xihu Sag has undergone three major tectonic evolutionary stages, including the rapid subsidence stage of the initial rift (early to late Eocene), the post-rift sagging stage (early Oligocene to late Miocene), and the post-rift stage during which the East China Sea shelf exhibited regional subsidence (Pliocene to present) (Yang *et al*., 2004). During these periods, several formations, including the Pliocene Baoshi formation (E_1m), Eocene Bajiaoting formation (E_2o), Eocene Pinghu formation (E_2p), Oligocene Huagang formation (E_3h), Miocene Longjing formation (N_1l), Miocene Yuquan formation (N_1y), Miocene Liulang formation (N_1ll), Pliocene Santan formation (N_2s), and Quaternary Donghai Group (Q*dh*) strata, were deposited. The total sedimentary thickness of these formations was more than 10000 m (Xie *et al*., 2018) (Fig.1c). With respect to proven reserves, the Huagang formation and Pinghu formation are the most important oil- and gas-producing layers. Further, approximately 90% of the oil and gas resources in the Xihu Sag have been produced from these formations (Su *et al*., 2013; Hao *et al*., 2018). One of the main oil and gas layers, the Huagang formation, is widely distributed within the study area. It has a thickness of 1000–2000 m and was deposited during the post-rift sagging stage. The formation primarily comprises terrestrial sedimentary rocks, including interbedded sandstone, mudstone, shale, and interlayered coal seams, with fluvial and delta facies (Hu *et al*., 2010; Hao *et al*., 2018).

3 Preliminary Analysis of the Problems and Determination of the Study Direction

A group of sand bodies of distributed underwater channel subfacies can be observed within the H3 and H4 sand groups of the M7 structure. In the H3 sand bodies, the permeabilities of the water and gas layers are $(0.31-1000)\times10^{-3}\,\mu m^2$ and $(0.04-12)\times10^{-3}\,\mu m^2$, respectively. In the H4 sand bodies, the permeabilities of the water and gas layers are $(0.06-100)\times10^{-3}\,\mu m^2$ and $(0.11-10)\times10^{-3}\,\mu m^2$, respectively. Inverted physical properties can be clearly observed within the H3 and H4 sand groups. According to previous studies, sedimentation and diagenesis are the processes affecting the physical properties of the reservoirs. Some of the factors associated with sedimentation include grain size compositions, sorting and matrix content, whereas those associated with diagenesis include compaction, dissolution and cementation. These factors were correlated with the permeability of the reservoir to investigate the main reasons for this unusual phenomenon.

Fig.2 demonstrates that the change of porosity in the well M7-4 is well correlated with the change of permeability in the both H3 and H4 sand groups, indicating that the inversion of physical properties can be mainly attributed to the inverted porosity. Further, no significant differences in the median particle size, apparent compaction rate and primary intergranular porosity can be observed between the two sides of the gas-water interface, indicating that these factors are not the main reasons for the inversion of the porosity. However, the changes of secondary porosity are almost perfectly correlated with the variations of total core porosity. Further, the number of secondary dissolution pores and the apparent dissolution rates in the water layer are considerably higher than those in the gas layer. In addition, the apparent cementation rate of the gas layer is considerably higher than that of the water layer. Furthermore, other external conditions, such as temperature and pressure, are not considerably different on the two sides of the gas-water interface (Fig.2). Therefore, they can be excluded as controlling factors. It can be speculated that the reaction conditions associated with the reservoir rock and underground fluid are different in the gas and water layers, resulting in a stronger dissolution effect and a weaker cementation effect in the water layer and stronger cementation and weaker dissolution in the gas layer. Therefore, the porosity of the water layer is considerably higher than that of the gas layer. In this study, water-rock reaction experiments were conducted to simulate the underground fluid environment and to confirm this hypothesis.

According to Liu (2018), the diagenetic stage of the Huagang formation as a reservoir in the Xihu Sag can be classified into three stages: a mid-diagenetic stage A_1, a mid-diagenetic stage A_2, and a mid-diagenetic stage B. There are four possible sources for acidic materials during stage A_1, including i) the large amount of humic acid produced in the source rock owing to the degradation of organic matters during the early diagenetic stage, ii) the carbonic acid that remained in the formation after the atmospheric freshwater leaching during the early stage, iii) the large amount of organic acid obtained by the breakdown of oxygen-containing groups under the action of chemical degradation that can be attributed to the effects of mineral oxidants and polysulfides during kerogen cracking, and iv) carbonic acid from the CO_2 generated by the oxidation of kerogen and other organic matters by the oxygen-containing groups dissolved in the fluids within the formation. An acidic environment was formed during mid-diagenetic stage A_1 because of the presence of these acids. The formation formed under an acidic environment can be identified based on several characteristics, including siliceous cementation, kaolinite cementation, and strong dissolution. At mid-diagenetic stage B, organic acids were destroyed and consumed because of the cracking and dissolution of minerals observed during the early stage. Further, the decarboxylation effect became weak and the supply of CO_2 reduced, considerably reducing the source of acidic materials. Simultaneously, the Ro of organic matter exceeded 1.3% and the fluid environment changed from acidic to alkaline (Tang *et al*., 2013), as indicated by calcareous cementation, illite aggregation, and quartz dissolution. The mid-diagenetic stage A_2 was the transitional period from an acidic environment to an alkaline environment between the mid-diagenetic stages A_1 and B, and the diagenetic

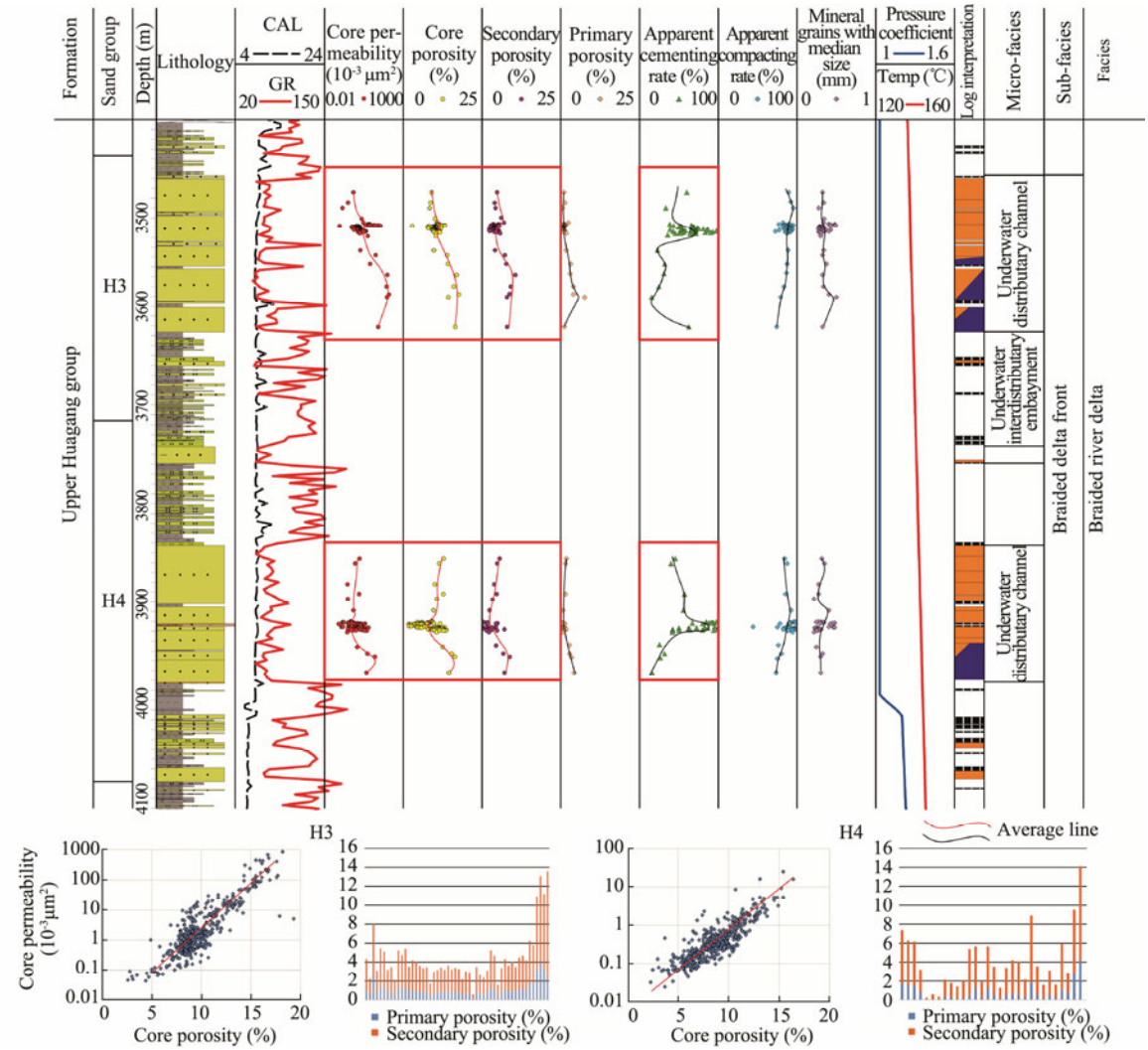

Fig.2 Variation of the physical properties and possible controlling factors for the H3 and H4 sand groups in well M7-4.

environment was approximately neutral during this stage. In addition, the maturity of primary organic matter in the same stratum can be used to identify the diagenetic environment (Ro=0.5%–0.7% at stage A_1; Ro=0.7%–1.3% at stage A_2; Ro>1.3% at stage B). Based on the results of the aforementioned studies and the burial history, thermal history, and thin-section data, the diagenetic environment at the mid-diagenetic stage of the M7 structure in the Huagang formation can be finely subdivided vertically (Fig.3). The depth of the acidic diagenetic environment at the mid-diagenetic stage A_1 is 2500–3630 m, whereas that of the transitional zone between the acidic and alkaline environments at the mid-diagenetic stage A_2 is more than 3630 m. Thus, the H3 sand bodies of the M7 structure in most wells were present in an acidic diagenetic environment, except for those at the bottom in the well M7-2, which were located in a transitional zone from acidic to alkaline environment. The diagenetic environment of the sand bodies in the H4 section is also transitional.

Based on the above results, the acidic fluid environment, which was mainly obtained because of organic acids and carbonic acid, the neutral fluid environment, and the alkaline fluid environment must be simulated to observe the changes of reservoir rocks under different fluid conditions.

4 Samples and Experimental Methods

Experimental samples were obtained from the section H3 of wells M7-1 and M7-4 (the depth of the sample is 3504–3630 m, the corresponding formation temperature is 137.50–139.10℃, the pressure is 32.51–35.57 Mpa, and the pressure coefficient is 1. The clastic particles mainly comprised quartz along with some feldspar and a small amount of lithic fragments. Localized quartz enlarement was observed even though it was not common. The surface porosity ranged from 13% to 15%, which is in the medium range. The dissolution pores and intergranular dissolution pores constituted 4.5% and 4.0% of the samples, respectively, and the remainders are primary pores. Kaolinite, illite and chlorite rims were commonly observed.

The original samples were cylinders with 2-cm diameters (Fig.4a). The samples were cut into several disks with the diameters of 2 cm and thicknesses of 2 mm to make it easier for the reaction liquid to enter the samples during the experiment (Fig.4b). Each disk was then broken into four pieces using small tweezers to ensure that each piece

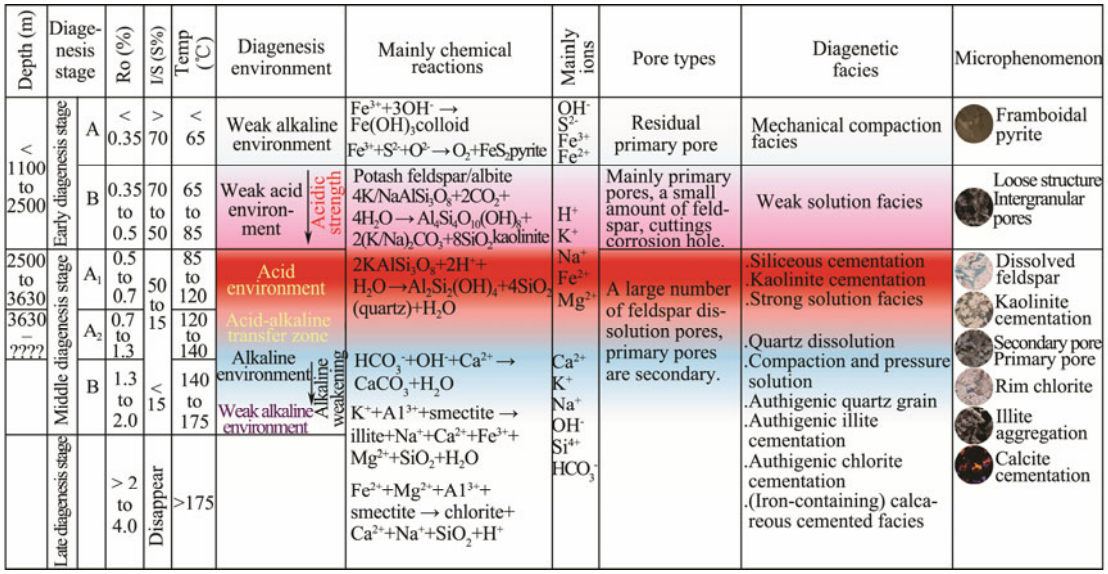

Fig.3 Vertical division of the diagenetic environment in the M7 structure (modified from Liu (2018), according to the actual conditions of the M7 structure).

had its natural fracture surfaces (Fig.4c; surface *s*). Subsequently, the samples were washed with purified water for 10 min using an ultrasonic cleaner to eliminate the debris and impurities produced during the cutting process. Finally, the samples were dried in an oven. Two of the four pieces (Fig.4c; (1) and (2)) for each small disk were used to represent the state prior to the experiment. The remaining two pieces (Fig.4c; (3) and (4)), which were selected to represent the state after the experiment, were placed in the reaction container. One piece was polished into a thin section to examine the variations in surface porosity and minerals, whereas the other piece was examined using a scanning electron microscope.

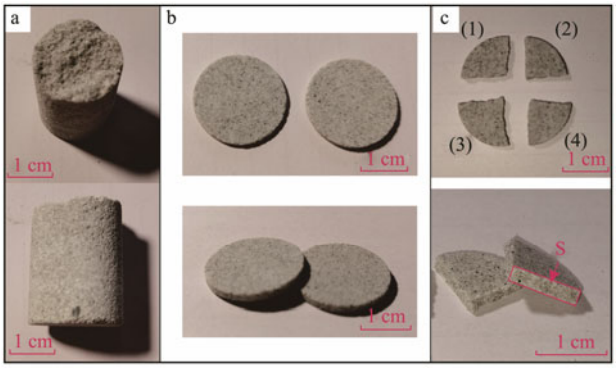

Fig.4 Experimental samples.

As part of this study, a high-temperature and high-pressure reactor was developed for using as the reaction vessel. The reactor had a capacity of 20 mL, and the temperature and pressure were controlled by the computer programs. The maximum temperature in the reactor was 400℃, and the maximum pressure was 30 MPa. The difference of the surface porosities before and after the simulation experiment was calculated, and the fracture surface was examined *via* scanning electron microscopy to observe the variations in minerals. In addition, the pH values of the reaction liquid before and after the reaction were recorded and compared. The reactions were conducted at different temperatures (60℃, 80℃, 100℃, 120℃, 140℃, 160℃, and 200℃) in the acetic acid solution, the CO_2 buffered solution, the purified water, and the NaOH solution.

In the experiments, the volume ratio of the rock sample to the reaction solution was approximately 113:1 and the reaction time was 100 h. Large numbers of bubbles attached to the surfaces of the samples under the high-temperature environment, causing the samples to move and even float upward, thereby disturbing the experimental reaction. After repeated attempts, we found when the pressure increased to 7.82 MPa under the experimental conditions, the bubbles disappeared. Therefore, the pressure was maintained at approximately 12 MPa. According to the engineering design principles, we set an allowance of 50%. using a program-controlled pressure device. In the CO_2 buffered solution reaction system, CO_2 was used for pressurization, and the remaining solutions were pressurized with helium gas. The pH values before and after the reaction were measured using a pH tester (enhanced version 3.0 of the pH tester produced by the Lianshi Instrument Co., Ltd., Jiangsu, China).

In addition to the aforementioned experiments, some positioning observation experiments were performed. In this procedure, a single sample was subjected to multiple experiments at different temperatures. After each experiment, the same position on the sample was observed using a scanning electron microscope to analyze the changes in the same mineral particles at different temperatures.

5 Results and Discussion

5.1 Organic Acid Reaction System

Surdam *et al.* (1984, 1989) proposed that the dissolution of organic acids in strata may produce secondary pores in

the rock. This view has been controversial because many scholars believe that acid dissolution is not sufficient to obtain a large number of dissolution pores (Bjorlykke *et al*., 1992; Giles *et al*., 1994). Herein, during the experiment in which the acetic acid solution was used, feldspar, calcite, and other alkaline minerals dissolved in the acid and the dissolution capacity gradually increased with the increasing temperature. At temperatures lower than 80℃, the carbonate minerals dissolved rapidly. However, the dissolution of feldspar could only be clearly observed at temperatures greater than 100℃ (Fig.5a). At 200℃, feldspar dissolved easily and almost all the feldspar particles were destroyed, leaving little residue (Fig.5b). Acid minerals, such as quartz, were not lost as the feldspar dissolved, but tended to increase. The dissolution of feldspar and the growth of quartz were observed during the experiments. Figs.5c and 5d show that the dissolution degrees of feldspar are different at different temperatures. Fine quartz particles grew in the pores produced by the dissolution of feldspar. Only fine granulated quartz particles remained after feldspar was completely dissolved. This may have been quartz cementation owing to the precipitation of the supersaturated silicates added in the solution during the dissolution of feldspar. In addition, the solution after the reactions became weakly alkaline (pH=7.7−8.9) at temperatures other than 60℃. In addition, the illitization of the feldspar particle surfaces could be observed in the acetic acid environment (Fig.5e). This process may consume the H^+ ions, resulting in a weakly alkaline reaction environment. Furthermore, the surfacze porosity of the samples increased to varying degrees at all temperatures. The highest increase was observed during the experiment conducted at 200℃ (by 17%) (Table 1).

5.2 CO_2 Reaction System

In the CO_2 reaction system, the dissolution of feldspar was gentle at temperatures lower than 120℃. Obvious dissolution could be observed in the experiments conducted at temperatures greater than 140℃ (Fig.5f). However, unlike the experiments conducted by using the acetic acid solution, the pH values did not change before and after the reactions. Because the CO_2 pressurization during the

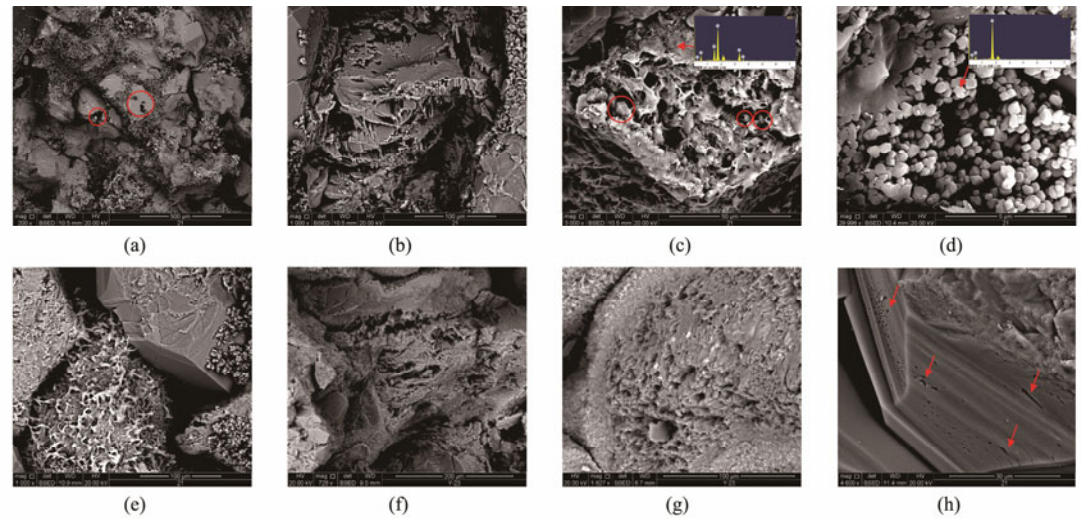

Fig.5 Scanning electron microscopy images of the samples under different experimental conditions. (a), dissolution pores found in feldspar particles after the sample reacted with an acetic acid solution at 120℃; (b), residual feldspar particles after dissolution in an acetic acid solution at 200℃; (c), growth of quartz particles in pores produced by the feldspar dissolution after the sample reacted with an acetic acid solution at 140℃; (d), growth of quartz particles after feldspar was completely dissolved in an acetic acid solution at 200℃ (photographed at the same position as the sample in Fig.c); (e), illitization on the surface of feldspar particles after reaction with an acetic acid solution at 120℃; (f), large number of dissolution pores were found in feldspar particles after reaction with a CO_2 solution at 140℃; (g), the small number of 'honeycomb' dissolution pores remained after reaction with purified water at 160℃; and (h), slight dissolution, occasionally observed on the surface of quartz particles after reaction with NaOH solution at 200℃.

Table 1 pH and surface porosity of the samples before and after the experiments

Experiment Temperature (℃)	Acetic acid solution		CO_2 buffered solution		Pure water		NaOH solution	
	pH	Surface porosity	pH	Surface porosity	pH	Surface porosity	pH	Surface porosity
60	4.03→7.67	15%→17%	5.88→5.97	13%→14%	7.05→7.15	14%→14%	11.15→11.20	15%→15%
80	4.11→7.92	15%→17%	6.12→5.85	15%→15%	7.07→7.03	15%→15%	10.99→11.09	15%→15%
100	3.66→8.38	14%→18%	5.52→5.90	14%→16%	7.00→7.24	15%→16%	11.07→11.02	15%→15%
120	3.98→8.77	15%→23%	6.31→6.02	14%→17%	7.10→7.24	13%→15%	11.34→11.09	14%→14%
140	3.79→8.66	15%→27%	5.46→6.34	16%→21%	7.02→7.77	16%→18%	11.34→11.18	15%→15%
160	3.93→9.02	15%→28%	6.43→6.28	15%→20%	7.12→8.03	13%→14%	11.32→11.03	14%→14%
200	3.57→9.57	15%→32%	5.77→5.97	15%→23%	7.03→8.18	15%→18%	11.23→10.89	15%→15%

reaction continuously supplied CO_2 to the solution, the H^+ ions were constantly supplemented when CO_2 was combined with the water molecules to form carbonic acid. Generally, the dissolution of the feldspar in the rocks could be clearly observed in the carbonate solution. The degree of dissolution was slightly low, and the increase in surface porosity was less than that observed in organic acid solution. However, in the experiments conducted at temperatures greater than 120℃, the increase of surface porosity was in a considerable range of 3%–7%。

5.3 Neutral Reaction System

The reaction of the rock samples in purified water was very slow compared with that in acidic environments. At temperatures of greater than 160℃, only a small number of honeycomb dissolution pores could be observed on the surface of feldspar particles (Fig.5g). The changes in acidic minerals, such as quartz and chlorite, were small and the increase in surface porosity was limited, with a maximum increase of only 3%. However, the solution still became weakly alkaline after the reactions, indicating that a weakly alkaline environment is the equilibrium environment for the dissolution of alkaline minerals.

5.4 Alkaline Reaction System

In the NaOH solution, the mixture of kaolinite and illite can be observed in the rock samples. However, there was little dissolution of large-grained minerals such as feldspar and quartz. During the experiments, the roughening of quartz grains with some sporadic pores was observed at 200℃ only (Fig.5h). Thus, under alkaline conditions, more extreme conditions are needed for mineral dissolution, and the formation of a large number of secondary pores are difficult. The surface porosity did not change considerably in this case.

6 Analysis of the Reasons for the Inverted Physical Properties in the M7 Structure

We collected a large amount of data about the M7 structure from two sets of sand bodies in the H3 and H4 members. Through comprehensive analysis, the inversion phenomena of physical properties were obvious in these two sets of sand bodies. However, there were obvious differences between them in the thicknesses of the formations with inverted physical properties, which had to be analyzed separately with the experimental results.

6.1 In Section H3 (Acidic Diagenetic Environment)

Fig.6 shows the permeability, apparent cementation rate, porosity, and secondary porosity of the sand bodies in the section H3 of each well in the M7 structure. The structure is divided into four intervals. The a_{H3} interval is a common gas layer (no special phenomena are observed away from the gas-water interface) and has a maximum depth of 3510 m. The b_{H3} interval ranges from 3510 to 3535 m in depth and belongs to the gas layer near the gas-water interface. When compared with the a_{H3} interval, the b_{H3} interval has a higher cementation rate, with quartz as the main cementing mineral. The b_{H3} interval exhibits the low porosity and belongs to the low-porosity gas layer. The c_{H3} interval occurs at the depth of 3535–3625 m. When compared with the b_{H3} interval, the c_{H3} interval exhibits considerably lower cementation rate and higher porosity, and the pore system is dominated by secondary porosity. The c_{H3} interval is a high-porosity water layer. The permeability and porosity of the d_{H3} interval are considerably lower than those of the c_{H3} interval and even lower than those of the a_{H3} interval. A comparison of the four intervals shows that the physical properties of the water layer

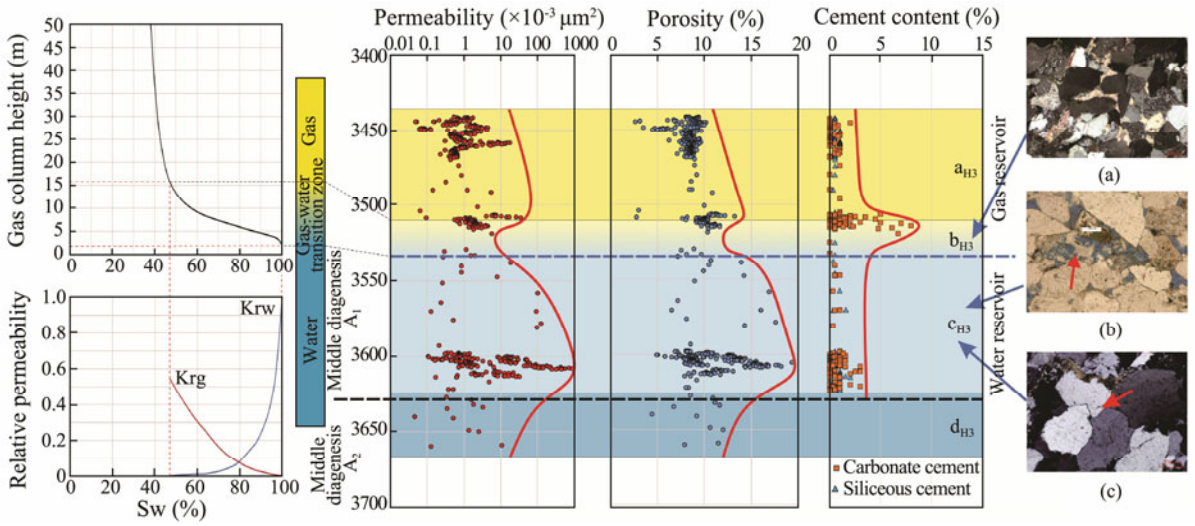

Fig.6 Permeability, porosity, and cementation rate of the sand bodies from the section H3 in the M7 structure. (a), carbonate cementation, M7-4, 3510.20 m (orthogonal polarization); (b), residual feldspar particles after the dissolution, M7-4, 3611.00 m (single polarization); and (c), secondary quartz enlargement and siliceous cementation, M7-3, 3564.20 m (cross polarization).

(the c_{H3} interval) are considerably better than those of the gas layer (the b_{H3} interval) as the reservoir, indicating that

the physical properties are inverted (Fig.6).

According to the diagenetic environment in the M7 structure, there are sufficient H^+ ions in solutions under the acidic diagenetic environment at the diagenetic stage A_1. Based on this experiment, both an organic acid solution and a CO_2 buffered solution can cause obvious dissolution of the alkaline minerals in rocks. Therefore, this can be considered as the main reason for the high porosity and permeability in the c_{H3} interval. In addition, both the permeability and porosity in the c_{H3} interval increase with depth, which may be due to the strong dissolution effect at high temperatures.

The contents of Ca^{2+} and HCO_3^- ion are high in the fluids in the c_{H3} interval because a large amount of feldspar has been dissolved. Due to the capillary pressure, a gas-water transition zone is formed with the decreasing in the height of the gas water interface. The fluid in the gas-water transition zone is connected with fluid in the water layer. Based on the experimental results of the capillary pressure test and the experimental data of water-driven gas displacement provided by CNOOC, the thickness of the gas-water transition zone in the section H3 was 15–22 m, which is consistent with the thickness of the b_{H3} layer (Fig.6). Thus, the b_{H3} layer may be the gas-water transition zone. The ions in c_{H3} layer may enter into the b_{H3} layer by diffusion because of the connectivity. Once these ions entered the b_{H3} layer, which exhibited water shortage and poor water fluidity, cementation could easily occur. This is the reason for the increase in the cementation rate and the poor physical properties in the b_{H3} layer. Although SiO_2 is generated during the dissolution of feldspar, it was difficult for SiO_2 to migrate into the gas layer along with the fluid because of the low solubility of SiO_2 in water. So majority of dissolved SiO_2 could only precipitate as quartz crystals *in situ*. Therefore, carbonate cementation is dominant in the b_{H3} interval, whereas siliceous cementation is dominant in the c_{H3} interval. This speculation is supported by experimental results, which indicate that the crystallization of quartz occurred after feldspar was dissolved by organic acids. The a_{H3} is a dry gas layer containing only a very small quantity of bound water. In addition, the Ca^{2+} and HCO_3^- ion-rich fluids cannot be transported to the a_{H3} layer because the bound water has been separated from the lower water body; therefore, the cementation rate in the a_{H3} layer cannot increase. Natural gas isolated the layer a_{H3} from groundwater; hence, layer a_{H3} did not participate in the water-rock reaction. Therefore, there was no special change in the physical properties of the a_{H3} layer.

The boundary between the d_{H3} and c_{H3} intervals is located at a depth of 3625 m, which is very close to the lower depth limit (3630 m) of the formation at diagenetic stage A_1 in the M7 structure. Therefore, the d_{H3} interval lies within the acid-alkaline transition zone at the diagenetic stage A_2, and the pH values increase gradually with the increasing depth. Thus, the dissolution ability of the fluid to the reservoir rocks is reduced, eventually causing the physical properties of the d_{H3} interval to become poor again. If the d_{H3} interval did not lie in the acid-alkaline transition zone, the degree of dissolution may continue to increase until the alkaline minerals were completely consumed.

Based on the morphology of the envelope, this inversion of physical properties is h-type. The precondition for the occurrence of this type of inversion is that the entire reservoir is under an acidic diagenetic environment and adequate H^+ ion can be supplied.

6.2 In the Segment H4 (Neutral Diagenetic Environment)

Similar to the sand body in the segment H3, the segment H4 can be divided into four depth sections (a_{H4}, b_{H4}, c_{H4}, and d_{H4}) based on the permeability, porosity, cementation rate, and secondary porosity. However, the depth of the c_{H4} interval (a high-porosity water layer) ranges from 3940 to 3975 m, with the thickness of only 35 m, which is considerably different from the c_{H4} interval (90 m) in the H3 sand body. Additionally, calcareous cementation was clearly observed in the b_{H4} interval, and siliceous cementation was observed in the c_{H4} interval (Fig.7).

According to the diagenetic environment in the M7 structure, the entire H4 sand body lies within the acid-alkaline transition zone at the diagenetic stage A_2 and the diagenetic environment is near-neutral or even weakly alkaline. In this case, dissolution was restricted to limited conditions. In the neutral reaction environment, only a small number of dissolution pores could be observed on the surface of minerals at temperatures lower than 160℃. In the alkaline environment, dissolution pores were occasionally observed only at the temperature of 200℃. The temperature of the segment H4 in the M7 structure is considerably lower than that required for the occurrence of dissolution. Therefore, the fluid in the water layer does not easily cause the formation of significant dissolution pores.

The gas-production testing results for the sand body in the H4 section of well M7-1 indicated that the CO_2 content in the natural gas was up to 5.8%, indicating that there was a source of acidic materials for the water-rock reactions. In the CO_2 reaction system in the experiments, H^+ ions were continuously supplied due to the dissolution of the CO_2 gas. Therefore, the pH value remained below 7 under all conditions. The pressure of the fluid in the segment H4 is considerably greater than the pressure used in the experiment (12 MPa). Thus, the necessary conditions required for the CO_2 in the gas layer to enter the water layer in a neutral environment were achieved. After CO_2 entered the water layer, the fluid near the gas-water interface became weakly acidic, resulting in appropriate conditions for the dissolution of alkaline minerals. Because the depth to which CO_2 can penetrate within the water layer was limited, the thickness of the c_{H4} interval was very small.

After the alkaline minerals were dissolved by the carbonate solution, the fluid in the water layer contained Ca^{2+} ions. Because the water layer was rich in water and CO_2, the following reaction that produced Ca^{2+} ions occurred.

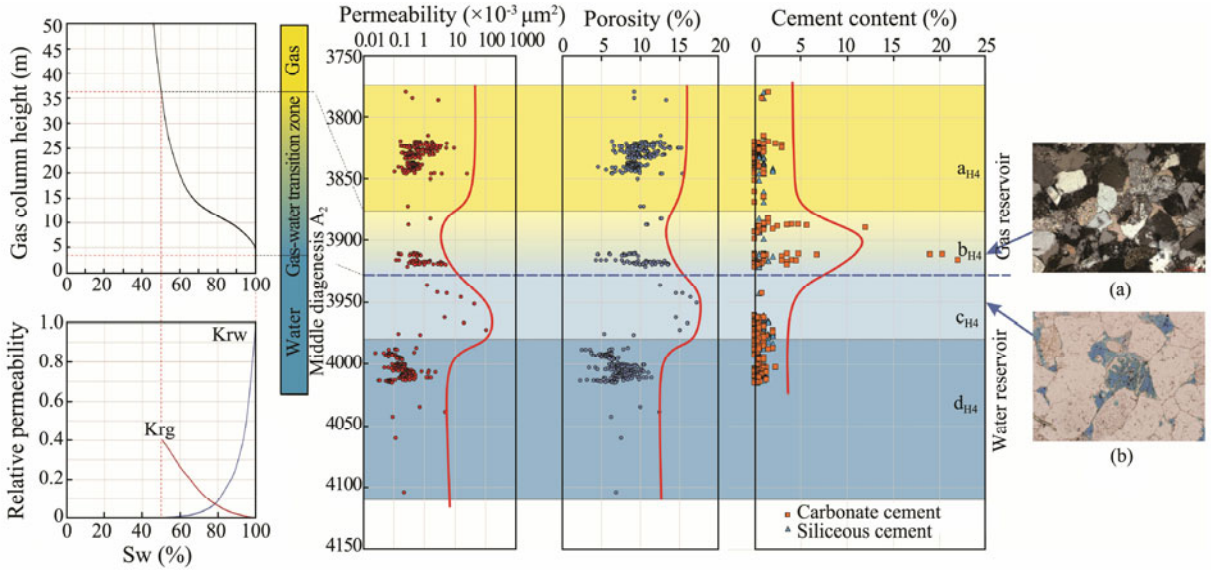

Fig.7 Permeability, porosity, and cementation rate of the H4 sand body in the M7 structure. (a), carbonate cementation, M7-4, 3916.10 m (orthogonal polarization); and (b), residual feldspar after dissolution, M7-2, 3964.20 m (single polarization).

$$CaCO_3 + H_2O\ (\text{large mass}) + CO_2 \rightarrow Ca(HCO_3)_2\,.$$

By analyzing the related experimental data in a manner similar to the sand bodies in the H3 member, the thickness of the gas-water transition zone in the H4 member was found to be 35−41 m. This is consistent with the thickness of the b_{H4} layer (Fig.7), which is poor in terms of physical properties but exhibit considerable cementation. The Ca^{2+} and HCO_3^- ions in the associated water body entered the b_{H4} layer *via* diffusion, providing a material basis for cementation in the layer. Because of the lack of water in the gas layer, the following reaction occurred and produced calcareous cementation in the b_{H4} segment.

$$Ca(HCO_3)_2 \rightarrow CaCO_3 + H_2O\ (\text{small number of}) + CO_2\,.$$

Although some of the SiO_3^{2-} ions are still present in the water, their concentration is considerably lower than that of the HCO_3^- ions. In addition, the neutral diagenetic environment is favorable to calcareous cementation. Therefore, calcareous cementation is dominant in the b_{H4} interval.

Based on the morphology of the envelope of the physical properties, the inversion of physical properties occurring near the gas-water interface has been labeled as S-type. The precondition for the occurrence of this type of inversion of physical properties is that the whole reservoir must have a neutral or weakly alkaline diagenetic environment and the acidic materials must originate from the gas layer.

7 Conclusions

1) The physical properties of the water layer in the Huagang formation in the Xihu Sag are better than those of the gas layer. This can be mainly attributed to the different chemical environments of the gas layer, transition zone, and water layer, and resultant different water-rock reactions. Thus, the physical properties are inverted. The particular sources of acids are the prerequisite for the occurrence of this phenomenon in the Huagang formation.

2) Because of differences in the sources of the acids, there are two different types of inversion for physical properties. In the first type, the acidic materials are sourced from the water layer. The secondary pores are well developed throughout the water layer, and the physical properties of the overall layer are more suitable for the gas migration and storage than those of the gas layer. This type can be observed under an acidic diagenetic environment (mid-diagenetic stage A_1). In the second type, acidic materials are sourced from the acidic gas originating from the gas layer, and only the water layer near the gas-water interface becomes acidic owing to the dissolution of the acidic gas. Therefore, the inversion of physical properties can be observed only near the gas-water interface. This phenomenon occurs in a diagenetic environment that tends to be neutral (the acid-alkaline transition zone at mid-diagenetic stage A_2).

3) These inversion phenomena may be the result of various factors, for example, differential compaction, hydrocarbon charging and migration, and alteration of special minerals. This study only discusses it as a diagenetic phenomenon based on previous research, which is also the limitation associated with our approach. Further studies about the remaining factors will be conducted in future.

Acknowledgement

This research was supported financially by the National Key Technology Research and Development Program of China during the '13th Five-Year Plan' (No. 2016ZX0502 7-002-006).

References

Bjorlykke, K., Nedkvitne, T., Ramm, M., and Saigal, G. C., 1992. Diagenetic processes in the Brent Group (middle Jurassic) reservoirs of the North Sea: An overview. *Geological Society*, **61** (1): 263-287.

Dai, L. M., Li, S. Z., Lou, D., Liu, X., Suo, Y. H., and Yu, S., 2014. Numerical modeling of late Miocene tectonic inversion in the Xihu Sag, East China Sea Shelf Basin, China. *Journal of Asian Earth Sciences*, **86**: 25-37.

Giles, M. R., Boer, R. B. D., and Marshall, J. D., 1994. How important are organic acids in generating secondary porosity in the subsurface? In: *Organic Acids in Geological Processes*. Springer, Berlin, 449-470.

Han, X. Q., Fang, T., Cao, J., Gao, H. L., Zhang, B., Zhang, L. K., *et al*., 2019. Simulation experiment of gas charging and gas-bearing change of tight sandstone reservoir of Shanxi formation in Yan'an gas field, Ordos Basin. *Natural Gas Geoscience*, **30** (12): 1721-1731 (in Chinese with English abstract).

Hao, L. L., Wang, Q., Guo, R. L., Tuo, C. G., Ma, D. X., Mou, W. W., *et al*., 2018. Diagenetic fluids evolution of Oligocene Huagang formation sandstone reservoir in the south of Xihu Sag, the East China Sea Shelf Basin: Constraints from petrology, mineralogy, and isotope geochemistry. *Acta Oceanologica Sinica*, **37** (2): 25-34.

He, F. Q., Rao, Y., Wang, W. H., and Wang, Y. H., 2020. Prediction of hydrocarbon reservoirs within coal-bearing formations. *Journal of Geophysics and Engineering*, **17** (3): 484-492.

Hu, M. Y., Ke, L., and Liang, J. S., 2010. The characteristics and pattern of sedimentary facies of Huagang formation in Xihu Depression. *Journal of Oil and Gas Technology*, **32** (5): 1-5 (in Chinese with English abstract).

Hu, W. S., Chai, H. D., Li, R. S., Xu, F., and Ge, H. P., 2010. Application of balanced section technique to the study of positive inversion structure and hydrocarbon accumulation control in Xihu Depression of East China Sea. *Special Oil & Gas Reservoirs*, **17** (1): 15-19 (in Chinese with English abstract).

Li, J. Y., Jiang, B., Qu, Z. H., Shi, Y., Xu, J., and Li, P., 2016. Tectonic evolution and control of coal in Donghai Xihu Sag. *Coal Geology & Exploration*, **44** (5): 22-27 (in Chinese with English abstract).

Li, S. Q., and Li, C. J., 2003. Analysis on the petroleum resource distribution and exploration potential of the Xihu Depression, the East China Sea. *Petroleum Geology & Experiment*, **25** (6): 721-728 (in Chinese with English abstract).

Li, Y., Chen, S. J., Wu, B. Y., Qiu, D., Lin, R. P., and Li, J. L., 2017. Controlling factors on complex gas-water distribution in Xu-6 tight sandstone gas reservoir in Guang'an area. *Xinjiang Petroleum Geology*, **38** (2): 198-203 (in Chinese with English abstract).

Liu, R. M., Sun, S. C., and Wang, D. D., 2019. Study on sedimentary system of Huagang formation in Xi Hu Depression. *Petrochemical Industry Technology*, **4**: 133-134 (in Chinese with English abstract).

Liu, Y., 2018. Genetic mechanism of deep high-quality reservoir in the Palaeogene Huagang formation of Xihu Sag in the East China Sea Basin. PhD thesis. Chengdu University of Technology.

Su, A., Chen, H. H., Cao, L. S., Li, C. H., Lei, M. Z., and Zhao, Y. T., 2014. Distribution and genesis of the secondary pore of Paleogene reservoir in Xihu Depression, Eastern Sea Basin. *Acta Sedimentologica Sinica*, **32** (5): 949-956 (in Chinese with English abstract).

Su, A., Chen, H. H., Wang, C. W., Li, P. J., Zhang, H., Xiong, W. L., *et al*., 2013. Genesis and maturity identification of oil and gas in the Xihu Sag, East China Sea Basin. *Petroleum Exploration and Development*, **40** (5): 558-565.

Surdam, R. C., Boese, S. W., and Grossey, L. J., 1984. The chemistry of secondary porosity: Part 2. Aspects of porosity modification. *AAPG Memoir*, **37**: 127-149.

Surdam, R. C., Crossey, L. J., Sven Hagen, E., and Heasler, H. P., 1989. Organic-inorganic interactions and sandstone diagenesis. *AAPG Bulletin*, **73** (1): 1-23.

Tang, X. P., Huang, W. H., Li, M., Dong, G. G., Wu, G., Wang, W. Y., *et al*., 2013. Diagenetic environment evolution of deep sandstones in the upper Es4 of the Palaeogene in Lijin Sag. *Earth Science - Journal of China University of Geosciences*, **38** (4): 843-852 (in Chinese with English abstract).

Taylor, T. R., Giles, M. R., Hathon, L. A., Diggs, T. N., Braunsdorf, N. R., Birbiglia, G. V., *et al*., 2010. Sandstone diagenesis and reservoir quality prediction: Models, myths, and reality. *AAPG Bulletin*, **94** (8): 1032-1093.

Wang, Q., Li, S. Z., Guo, L. L., Suo, Y. H., and Dai, L. M., 2017. Analogue modelling and mechanism of tectonic inversion of the Xihu Sag, East China Sea Shelf Basin. *Journal of Asian Earth Sciences*, **139**: 129-141.

Xie, G. L., Shen, Y. L., Liu, S. G., and Hao, W. D., 2018. Trace and rare earth element (REE) characteristics of mudstones from Eocene Pinghu formation and Oligocene Huagang formation in Xihu Sag, East China Sea Basin: Implications for provenance, depositional conditions and paleoclimate. *Marine and Petroleum Geology*, **92**: 20-36.

Yang, F. L., Yu, H. X., Zhang, Q. L., and Li, Q. Y., 2009. Correlations between shortening rate, uplift rate, and inversion rate in central inversion zone of Xihu Depression, East China Sea Basin. *Journal of Earth Science*, **20** (4): 699-708.

Yang, S. C., Hu, S. B., Cai, D. S., Feng, X. J., Chen, L. L., and Gao, L., 2004. Present-day heat flow, thermal history and tectonic subsidence of the East China Sea Basin. *Marine and Petroleum Geology*, **21** (9): 1095-1105.

Zeng, J. H., and Wang, H. Y., 2000. Experimental study on oil migration and accumulation in the heterogeneous sand beds of different porosity and permeability. *Journal of the University of Petroleum, China*, **24** (4): 108-112 (in Chinese with English abstract).

Zhang, S. L., Zhang, J. P., Tang, X. J., and Zhang, T., 2014. Geometry characteristic of the fault system in Xihu Sag in East China Sea and its formation mechanism. *Marine Geology & Quaternary Geology*, **34** (1): 87-94 (in Chinese with English abstract).

Zhou, R. Q., Fu, H., Xu, G. S., Miao, Q., and Fu, Z. Q., 2018. Eocene Pinghu formation–Oligocene Huagang formation sequence stratigraphy and depositional model of Xihu Sag in East China Sea Basin. *Acta Sedimentologica Sinica*, **36** (1): 132-141 (in Chinese with English abstract).

(Edited by Chen Wenwen)